

Accelerating the Averaging Rate of Atomic Ensemble Clock Stability using Atomic Phase Lock

Nobuyasu Shiga^{1,2}, Michiaki Mizuno², Kohta Kido¹, Piyaphat Phoonthong^{2,3}, Kunihiro Okada⁴

¹ PRESTO, Japan Science and Technology (JST), 4-1-8 Honcho Kawaguchi, Saitama 332-0012, Japan

² National Institute of Information Communication and Technology, 4-2-1 Nukui-kitamachi, Koganei, Tokyo 184-8795, Japan

³ National Institute of Metrology Thailand (NIMT), 3/4-5, Moo 3, Klong 5, Klong Luang, Pathumthani, 12120 Thailand

⁴ Department of Physics, Sophia University, 7-1 Kioicho, Chiyoda-ku, Tokyo 102-8554, Japan

E-mail: shiga@nict.go.jp

Abstract. We experimentally demonstrated that the stability of an atomic clock improves at fastest rate τ^{-1} (where τ is the averaging time) when the phase of a local oscillator is genuinely locked to the continuous phase of atoms (atomic phase lock). For this demonstration, we developed a simple method that repeatedly monitors the atomic phase while retaining its coherence by observing only a portion of the whole ion cloud. Using this new method, we measured the continuous phase over 3 measurement cycles, and thereby improved the stability scaling from $\tau^{-1/2}$ to τ^{-1} during the 3 measurement cycles. Compared with the standard method that initialize phase during each measurement cycle, the long term stability was improved by a factor of $\sqrt{n_{cp}}$ (where n_{cp} is the number of continuous phase measurements). This simple method provides a path by which atomic clocks can approach a quantum projection noise limit, even when the measurement noise is dominated by technical noise.

1. Introduction

Much effort has been invested in improving the stability of atomic clocks, which were first demonstrated more than 50 years ago [1]. The stability of a clock, denoted by σ_y (where y is a fractional frequency), is expressed as [2]

$$\sigma_y = \frac{1}{K \cdot Q \cdot \text{SNR} \cdot \sqrt{n}} = \frac{1}{K \cdot Q \cdot \text{SNR}} \sqrt{\frac{T_c}{\tau}} \quad (1)$$

where K is a constant of the order unity that depends on the spectrum shape, Q is the quality factor, SNR is the Signal-to-noise ratio, and n is the total number of measurements. T_c and τ denote the cycle time and total measurement time, respectively. This description of clock stability, hereafter the SNR limit, improves the clock stability with $\tau^{-1/2}$ scaling. When the measurement noise is sufficiently suppressed and the SNR

is limited by quantum projection noise (QPN), the QPN replaces the SNR in Eq. (1); this is hereafter referred to as the QPN limit. From Eq. (1), we observe that stability can be improved by 1) increasing the Q of the resonance by increasing the probing time or carrier frequency, 2) increasing the SNR, and 3) averaging over many measurements (i.e., increasing the n). Past improvements have focused on strategies 1) and 2). For example, the Q of the optical ion clock developed by Bergquist et al. [3] was several orders of magnitude higher than that of microwave clocks. Katori et al. [4] demonstrated an optical lattice clock that simultaneously increases the Q and SNR. Squeezed [5] or entangled states [6] were proposed to improve the SNR, reducing the measurement noise to below the QPN limit [7]. However, Eq. (1) does not account for the effect of the dead time, known as the Dick effect [8]. The dead time is the time expended in any process other than probing the atom with microwaves. The stability reaches the Dick limited when it is limited by the frequency noise of the LO the dead time is significant. In this case, reducing the dead time reduces the σ_y by $\sigma_y \propto \tau^{-1}$ until the SNR limit line is reached (blue broken line in Figure 1 (a)). This idea [9] has been recently demonstrated [10].

To accelerate the averaging rate of strategy 3), we have proposed an atomic phase lock (APL) [11]. Principally, the atomic phase lock lowers the stability at fastest rate τ^{-1} , by genuinely monitoring the phase of the atom. Provided that the atomic phase remains coherent and is monitored as such, the stability of the atomic clock should improve by τ^{-1} . However, the stability of atomic clocks normally improves by $\tau^{-1/2}$ even when employing the Ramsey sequence [12], which measures the atomic phase. This trend occurs because the atomic phase is destroyed (and initialized) after each projection measurement cycle. If the atoms could maintain its phase coherence over many measurement cycles, the stability would reduce much more rapidly (as τ^{-1}), and the stability could be expressed as

$$\sigma_y^{APL} = \frac{1}{K \cdot Q \cdot \text{SNR} \cdot n} \sim \frac{1}{K \cdot f_0 \cdot \text{SNR} \cdot \tau}. \quad (2)$$

where σ_y^{APL} is the frequency stability under maintenance of the atomic phase coherence.

Figure 1 a) shows the typical stability of an atomic clock that is limited by LO noise. In the presence of significant dead time, its best stability is the Dick limit [8].

The APL permits stability below the SNR limit if the atomic phase is continuously monitored with negligible decoherence. To observe the τ^{-1} dependence due to APL, different from eliminating the dead time as mentioned above, our experiment was performed in a regime in which the measurement noise far exceeded the free-run LO noise. The situation is illustrated in Figure 1 b). In this limit, the stability is not improved by eliminating the dead time, but is improved by APL.

The present paper demonstrates the APL. Section 2 describes our experimental setup. We used a single ensemble of ions, and performed projection measurements on only a portion of the ions at a time (Section 3). Section 4 shows the results of three phase measurements obtained by the proposed method without resetting the atomic states. The stability is reduced by τ^{-1} instead of $\tau^{-1/2}$ and the long term stability line is

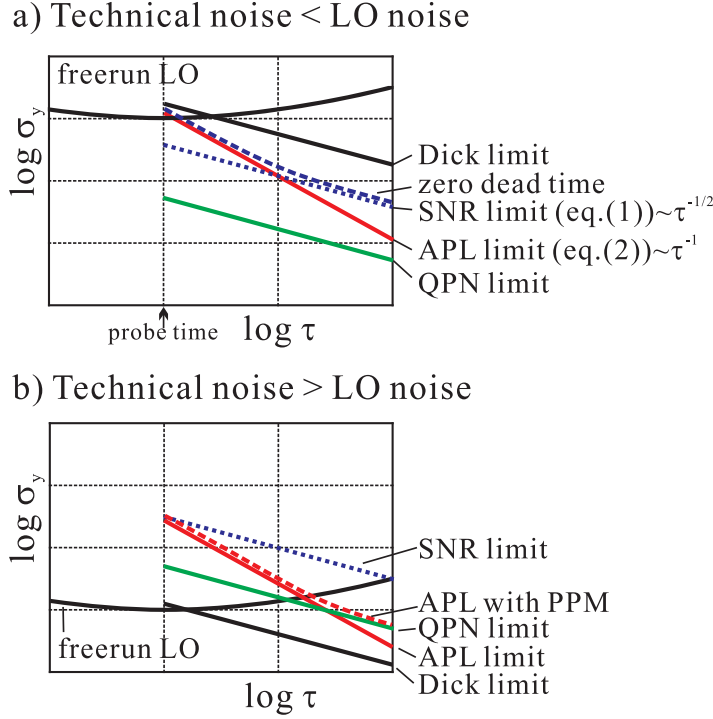


Figure 1. Typical stability of free-running LO and passive atomic clock. On both axes, the grid lines indicate decades. Signal-to-noise ratio (SNR) and atomic phase lock (APL) limits are given by Eq.(1) and Eq.(2), respectively. a) LO noise exceeds the technical noise. Free-running LO noise is larger than the SNR limit at $\tau = T_c$. Starting from the free-running noise, σ_y decreases at rate τ^{-1} until it reaches the SNR limit (blue dotted line). APL follows the same slope but is not limited by the SNR limit. b) Technical noise exceeds the LO noise. Since the Dick limit is negligible in this case, the APL alone is responsible for the τ^{-1} dependence.

lowered by a factor of $\sqrt{3}$ as expected. Section 5 applies the method and suggests ideas for further improvements.

2. Experimental setup

2.1. Ion trap

This section describes our experimental setup. Figure 2 shows our linear radio frequency (rf) quadrupole trap, in which four cylindrical rods (diameter= 2 mm) are placed at the corner of a square separated by 4 mm (center to center) and the DC bias plates are spaced by 30 mm. Sinusoidal voltage of 10.15 MHz with amplitude 330 V_{pp} and constant 50 V are applied on rf rods and DC bias plates, respectively. Ytterbium ions of 171 isotope (¹⁷¹Yb⁺) are selectively trapped by a 399 nm photo-ionization laser (not shown in Figure 2) and a 370 nm cooling laser.

Unintentionally, ions were trapped in two locations, delineated by red ovals in

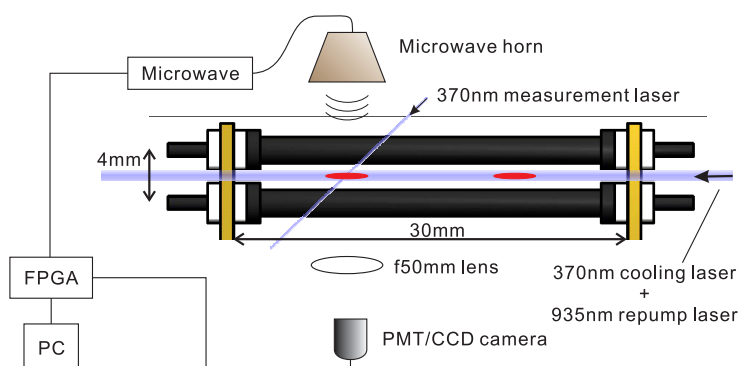


Figure 2. Schematic diagram of ion trap and measurement system. Ion clouds are indicated with red oval.

Figure 2. Each cloud (3 mm length) contains about 2000 ions. Finite element method simulations revealed that our rf rods are much more closely spaced than the distance between two bias plates. At such small separation, the DC electric near the trap center is shielded by the rods. Consequently, a small potential barrier (whose origin is unclear) remains in the center even with 50 V DC potential on the bias plates. One of the clouds was used for clock measurements.

2.2. Ion Cooling

Once trapped, the ions are cooled to about 50 mK by Doppler laser cooling. This 50 mK temperature was obtained by separately measuring the 370nm cooling transition broadening[13]. The ions were predominantly cooled by the 370 nm laser (13 μ W) and the cooling cycle was closed by combining the 935 nm repump laser (6 mW) with 14GHz modulation of the 370 nm cooling laser [14] (Figure 3). The trap area of the vacuum

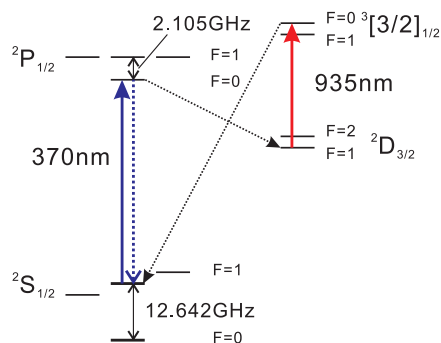


Figure 3. Simplified energy level diagram of $^{171}\text{Yb}^+$.

chamber was covered by a single layer magnetic shield of shielding factor 15, yielding an interior field of 0.04 Gauss. During microwave proving, this residual field was canceled

by 3 pairs of Helmholtz coils. The dark states were destabilized[15] by a 0.4 Gauss field tilted 45° from the laser axis, using the Helmholtz coils. The ions were initialized to the $^2S_{1/2}(F = 0)$ state by a cooling laser phase-modulated at 2.1GHz by an electro optical modulator.

2.3. Microwave transition

The 12 GHz microwave clock transition is the hyperfine splitting of the ground state. The ions were coupled to microwaves emitted by a microwave horn. The 12GHz microwave synthesizer was referenced to a hydrogen maser, and the synthesizer can be switched between two phase profiles (in our case, between 0° and 90°) using external logic. Microwave emission was terminated by a 60 dB isolation PIN switch.

The population ratio of the ions in the excited state ($^2S_{1/2}(F = 1, m_f = 0)$) was measured by the electron shelving technique[16], using the 370 nm laser without 14 GHz modulation.

Timings of switching lasers, microwave amplitude and phase, 14 GHz modulation and 2 GHz modulation of the cooling laser were precisely controlled by field programable gated array (FPGA). The FPGA also counted the number of photons, and passed the data to PC for further data processing.

3. APL via partial projection measurement

3.1. Partial projection measurement

We now introduce partial projection measurement (PPM). In PPM, a 16 μ W diagonal laser is operated at 370 nm (see Figure 2) such that only a portion of the ions interacts with the laser. The waists of the ions and diagonal beam are equal (approximately 200 μ m). The basic measurement sequence is as follows.

- (i) Initialize atomic state (cooling and pumping to $^2S_{1/2}(F = 0)$).
- (ii) Manipulate state with microwaves (details are shown in Figures 4 and 5)
- (iii) Perform PPM
- (iv) repeat steps (ii)-(iii).

After the first partial measurement, the projected ions became mixed with un-projected ions during manipulation period prior to the next measurement. We note that our ion temperature was sufficiently high enough such that the ion cloud never crystalized. The measured population is valid provided that the ratio of un-projected to projected ions exceeds the SNR of the measurement.

3.2. Check of PPM with Rabi oscillation signal

The validity of PPM was tested by first measuring the Rabi oscillation under PPM. This test evaluates whether PPM can correctly measure a population that is

constantly changed by microwave interaction. Figure 4 a) shows the measurement sequence of normal Rabi oscillations obtained under PPM. In standard Rabi oscillation

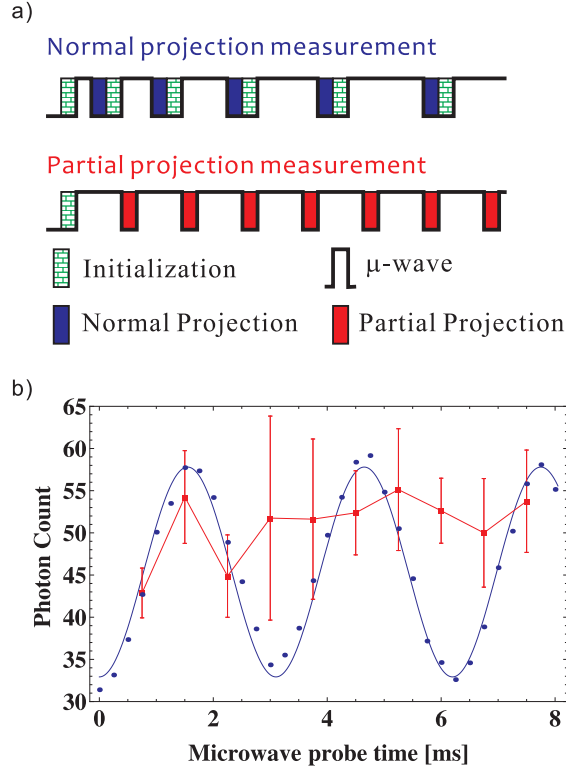


Figure 4. a) Sequence of normal projection measurement and PPM. b) Cases in which the ion state is re-initialized and not re-initialized after each measurement are shown in blue and red, respectively. Filled blue circles are the averages of 10 measurements. Solid line is a sinusoidal fitting. Filled red squares are the averages over 8 measurements. The error bars represent the standard deviations in a single measurement.

measurement, the atomic state is reset after each measurement cycle, and the probe time is increased at each cycle. In the PPM approach, the atomic state is not reset, rather another rotation is added in each cycle. The measured result is shown in Figure 4 b). If PPM is valid, the red data should align with the blue sinusoidal curve. We observe that PPM is correct up to three measurements, but desynchronizes from the correct population at and beyond the 4th measurement. This decoherence is discussed in the next chapter.

3.3. Check of PPM with continuous phase measurement (modified Ramsey method)

We now test the PPM in phase measurement sequences. To monitor the total phase difference accumulated over multiple measurement cycles, we must modify the Ramsey sequence as well as the projection measurement. Our modified Ramsey sequence is shown in Figure 5 a) and proceeds via the following steps: Basic sequence is,

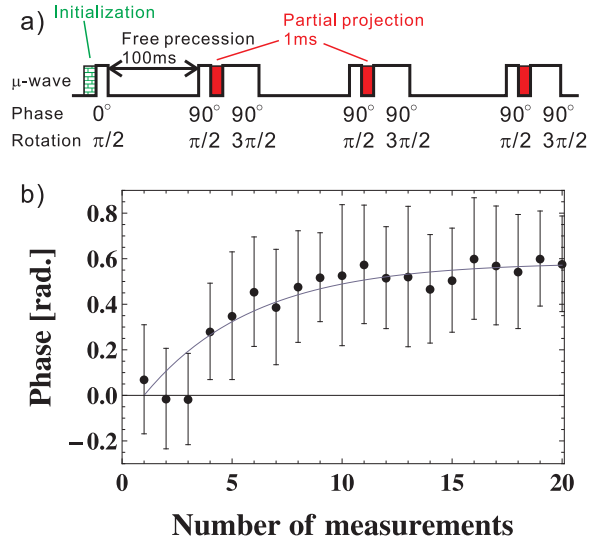


Figure 5. a) Sequence of continuous phase measurement with PPM. b) Continuous phase measurement (up to 20 PPM) with diagonal laser beam. Filled circles are averaged over 32 samples and error bar indicate the standard deviation.

- (i) Initialize once at the beginning of the measurement,
- (ii) Construct a superposition state by applying a $\pi/2$ rotation (0.75 ms) with 0° phase,
- (iii) Wait for a free precession time,
- (iv) Transfer the phase to the population by applying a $\pi/2$ rotation with 90° phase,
- (v) Perform PPM,
- (vi) Revert the population to the original phase by applying a $3\pi/2$ rotation with 90° phase.
- (vii) repeat (iii) ~ (vi).

This sequence is very similar to that proposed in our previous paper [11], but is slightly modified to accommodate technical limitation. Our 12GHz signal generator can switch phase with the external logic control in only two profiles (in our case, at 0° and 90°), so the $1/2\pi$ rotation at the 270° phase was replaced with a $3/2\pi$ rotation at the 90° . The 12 GHz microwave signal generator was referenced to a hydrogen maser, and the frequency noise was much smaller than the SNR of the measurements. The phase error in a hydrogen maser at 0.1 s averaging time is below 0.02 radians. This implies that the measured zero phase shift between the LO and atoms should always lie within the measurement noise. Figure 5 b) shows the measured phase over 20 PPM measurements. Each datum is the average of 32 measurements and measurement noise (~ 0.2 radians) is mainly due to scattering of the 370nm laser. Clearly, PPM measures the correct phase over three consecutive measurements, and thereafter deviates from the true phase by more than one sigma. After the 3rd measurement, the atomic phase is abruptly loses coherence and the population ratio rapidly asymptotes toward 70% excitation. Together

with the Rabi oscillations measured by PPM, we conclude that our continuous phase measurement is valid up to three measurements.

We consider a simple model, in which a constant number of ions are projected and lose coherence during each measurement. Prior to the n -th measurement, the proportion of ions whose states are projected, denoted as P_{proj} , is given by,

$$P_{proj} = 1 - (1 - p)^{n-1} \quad (3)$$

where p is the number of ions get projected in a single measurement, normalized by the total number of ions. Fitting the data in Figure 5 to Eq. (3) and an additional fitting parameter (the amplitude) yields the solid curve in Figure 5. From this fitting, p is estimated as 18 %.

3.4. Simulation evaluation of PPM

To elucidate the decoherence rate, we simulated the ion motions using a molecular dynamics method[17]. We calculated the motions of 2000 ions trapped in a potential that corresponding to our trap parameters, assuming constant temperature. We confirmed that ions undergo Brownian motion with a mean-squared displacement along the optical axis $\Delta z^2 \equiv \langle (z - z_0)^2 \rangle$ (where z_0 is the initial position at $t = 0$), given by

$$\Delta z^2 = 2Dt \quad (4)$$

where D is the diffusion constant of ions and t denotes time.

Simulating this ensemble with $T=50$ mK, we obtained $D = 3.5 \times 10^{-6}[m^2s^{-1}]$. Varying the temperature from 10 mK to 2 K, we found that D and T were related through the Boltzmann constant and the mobility μ , namely,

$$D = \mu k_B T. \quad (5)$$

The fitting gives $\mu = 8.62 \times 10^{18}[m^2s^{-1}J^{-1}]$.

Next, we counted the number of ions passing through the region in which the diagonal laser and ions overlap. At $T = 50$ mK, 17 % of the total ions were struck by the measurement laser within 1 ms. This implies that 17 % of the ions were projected and decohered during 1 ms measurement time, consistent with the estimates of Figure 5. The cause of the abrupt decoherence after the 3rd measurement remains unclear.

4. Allan deviation of APL based atomic clock

This section experimentally compares the stability of the standard method (in which phase is initialized during each cycle) with that of APL. APL initializes the phase after each sequence of 3 PPMs, as shown in Figure 6 a). Figure 6 b) shows the standard deviation in the APL results (filled red squares) and the overall Allan deviation (filled red triangles). APL ($\tau = 0.1 \sim 0.3$) and APL repetition ($\tau > 0.3$) are calculated in different ways. For $\tau = 0.1 \sim 0.3$, Δf is estimated as,

$$\Delta f = \frac{\Delta \phi_n}{nT_{FP}} \quad (6)$$

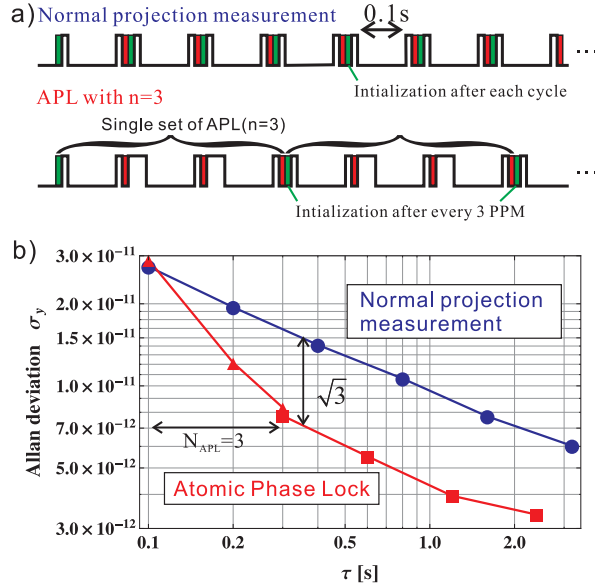


Figure 6. Standard deviation (red filled triangles) in the APL measurements and the Allan deviation (red filled squares) in the 3rd measurement of APL cycles. Allan deviations of the regular projection measurements (blue filled circles) are also shown.

where n indicates the n -th APL measurement cycle ($n = 1, 2, \text{ or } 3$). In Figure 6 b), the standard deviation in the n -th measurement scales as τ^{-1} . For $\tau > 0.3$, APL cycles are established, and we calculate and plot the Allan deviation from the final (3rd) measurement in each cycle. The triangles and circles in Figure 6 b) are calculated from the same data and the slight mismatch at $\tau = 0.3\text{s}$ is due to the difference between the standard and Allan deviations.

For comparison, the Allan deviation of the regular Ramsey measurement, in which the phase is initialized during each cycle, is also plotted in Figure 6 b). This deviation scales as $\tau^{-1/2}$. Based on the measured Allan deviations, the stability of APL is improved by a factor of $\sqrt{3}$, relative to the standard Ramsey cycles. Overall, we have demonstrated that APL improves the stability by a factor of $\sqrt{n_{CP}}$, where n_{cp} is the number of continuous APL measurement.

The number of valid PPMs can be increased by 1) reducing the temperature of the ions (lowering the Diffusion coefficient), 2) trapping more ions (reducing the proportion of the decohered ions in a single measurement), or 3) adopting weak measurements. We expect that this last strategy can greatly increase the number of valid PPM. A promising weak measurement is Faraday Rotation, discussed in detail in our previous paper[11].

5. Discussion

The method presented in this paper is useful when the performance of an atomic clock is limited by technical noise[7]. In the past, trapping more atoms more than the $(\text{SNR})^2$

was futile. However, APL via PPM enables the trapping of more number of atoms than $(\text{SNR})^2$, thereby lowering the stability line in Figure 1 to

$$\sigma_y = \frac{1}{\sqrt{n_{cp}} K \cdot Q \cdot \text{SNR}} \sqrt{\frac{T_c}{\tau}}. \quad (7)$$

PPM limits the n_{cp} to $N_{atom}/(\text{SNR})^2$ (where N_{atom} is the total number of atoms in the trap) because the number of measured atoms is adjusted to $(\text{SNR})^2$ and all of these atoms become decohered during a single measurement. When $n_{cp} = n_{atom}/(\text{SNR})^2$, Eq. (7) computes the QPN limit line. Therefore, when APL is based on PPM, the system cannot be improved beyond the QPN limit (Figure 1), except perhaps by weak measurement. However, discussion of the weak measurement limit is beyond the scope of this paper.

Recently, use of multiple atomic traps has been proposed [18, 19]. This scheme shows the same τ^{-1} scaling and an overall gain of $m2^{-m}$, where m is the number of atomic traps. Further stability improvements are conceivable if this scheme could be combined with APL.

Acknowledgments

This work was supported by the JST PRESTO program and NICT. We thank H. Hachisu and T. Ido for comments on this manuscript.

References

- [1] L. Essen and J. V. L. Parry: Nature **176** (1955) 280.
- [2] F. Riehle: *Frequency Standards: Basics and Applications* (Wiley-VCH, Weinheim, 2004) Chap. III.
- [3] S. A. Diddams, Th. Udem, J. C. Bergquist, E. A. Curtis, R. E. Drullinger, L. Hollberg, W. M. Itano, W. D. Lee, C. W. Oates, K. R. Vogel, and D. J. Wineland: Science **293** (2001) 825.
- [4] M. Takamoto, F. Hong, R. Higashi, and H. Katori: Nature **435** (2005) 321.
- [5] D. J. Wineland, J. J. Bollinger, W. M. Itano, F. L. Moore, and D. J. Heinzen: Phys. Rev. A **46** (1992) 6797.
- [6] J. J. Bollinger, W. M. Itano, D. J. Wineland, and D. J. Heinzen: Phys. Rev. A **54** (1996) 4649.
- [7] W. Itano, J. C. Bergquist, J. J. Bollinger, J. M. Gilligan, D. J. Heinzen, F. L. Moore, M. G. Raizen, and D. J. Wineland: Phys. Rev. A **47** (1993) 3554.
- [8] G. J. Dick: Proc. 19th Precise Time and Time Interval, 1987, p. 133.
- [9] G. J. Dick, J. D. Prestage, C. A. Greenhall, and L. Maleki: Proc. 22nd Precise Time and Time Interval, 1990, p. 487.
- [10] G. W. Biedermann, K. Takase, X. Wu, L. Deslauriers, S. Roy, and M. A. Kasevich: Phys. Rev. Lett. **111** (2013) 170802.
- [11] N. Shiga and M. Takeuchi: New J. Phys. **14** (2012) 023034.
- [12] N. F. Ramsey: *Molecular Beams* (Clarendon Press, Oxford, 1956) Chap. V.
- [13] P. Phoonthong, M. Mizuno, K. Kido, and N. Shiga: in preparation for publication.
- [14] S. M. Olmschenk: PhD. Thesis, University of Michigan (2009)
- [15] D. J. Berkeland and M. G. Boshier: Phys. Rev. A **65** (2002) 033413.
- [16] W. Nagourney, J. Sandberg, and H. Dehmelt: Phys. Rev. Lett. **56** (1986) 2797.
- [17] K. Okada, T. Takayanagi, M. Wada, S. Ohtani, and H. A. Schuessler: Phys. Rev. A **81** (2010) 013420.

- [18] J. Borregaard and A. S. Sørensen: Phys. Rev. Lett. (2013) 090802.
- [19] T. Rosenband and D. R. Leibbrandt: arXiv:1303.6357.